

# DEFINE YOUR FLOW




Own the direction of your research with the trailblazing ZE5™ Cell Analyzer

30-parameter analysis, unmatched sample flexibility, and easy to learn and use Everest™ Software now give both novice and expert users the power to set their own pace for discovery.

Visit us at [bio-rad.com/info/DefineYourFlow](http://bio-rad.com/info/DefineYourFlow)

**BIO-RAD**

## Gene-Edited Human Kidney Organoids Reveal Mechanisms of Disease in Podocyte Development

YONG KYUN KIM,<sup>a,b,c,d,\*</sup> IDO REFAELI,<sup>e,f,\*</sup> CRAIG R. BROOKS,<sup>g,\*</sup> PEIFENG JING,<sup>h</sup> RAMILA E. GULIEVA,<sup>a,b,c,d</sup> MICHAEL R. HUGHES,<sup>e,f</sup> NELLY M. CRUZ,<sup>a,b,c,d</sup> YANNAN LIU,<sup>h</sup> ANGELA J. CHURCHILL,<sup>a,b,c,d</sup> YULIANG WANG,<sup>c,i</sup> HONGXIA FU,<sup>c,d,j,k</sup> JEFFREY W. PIPPIN,<sup>a,d</sup> LIH Y. LIN,<sup>h</sup> STUART J. SHANKLAND,<sup>a,d</sup> A. WAYNE VOGL,<sup>l</sup> KELLY M. MCNAGNY,<sup>e,f</sup> BENJAMIN S. FREEDMAN <sup>a,b,c,d</sup>

**Key Words.** Pluripotent stem cells • Kidney • Adhesion receptors • Differentiation • Gene targeting • Developmental biology • Focal segmental glomerulosclerosis • Nephrogenesis • Cell adhesion • Foot processes • Slit diaphragm • Podocalyxin • Nephron • Podocin • Genome editing • Biophysics

### ABSTRACT

A critical event during kidney organogenesis is the differentiation of podocytes, specialized epithelial cells that filter blood plasma to form urine. Podocytes derived from human pluripotent stem cells (hPSC-podocytes) have recently been generated in nephron-like kidney organoids, but the developmental stage of these cells and their capacity to reveal disease mechanisms remains unclear. Here, we show that hPSC-podocytes phenocopy mammalian podocytes at the capillary loop stage (CLS), recapitulating key features of ultrastructure, gene expression, and mutant phenotype. hPSC-podocytes in vitro progressively establish junction-rich basal membranes (nephron<sup>+</sup>podocin<sup>+</sup>ZO-1<sup>+</sup>) and microvillus-rich apical membranes (podocalyxin<sup>+</sup>), similar to CLS podocytes in vivo. Ultrastructural, biophysical, and transcriptomic analysis of podocalyxin-knockout hPSCs and derived podocytes, generated using CRISPR/Cas9, reveals defects in the assembly of microvilli and lateral spaces between developing podocytes, resulting in failed junctional migration. These defects are phenocopied in CLS glomeruli of podocalyxin-deficient mice, which cannot produce urine, thereby demonstrating that podocalyxin has a conserved and essential role in mammalian podocyte maturation. Defining the maturity of hPSC-podocytes and their capacity to reveal and recapitulate pathophysiological mechanisms establishes a powerful framework for studying human kidney disease and regeneration. *STEM CELLS* 2017; 00:000–000

### SIGNIFICANCE STATEMENT

Human pluripotent stem cells (hPSCs) have recently been differentiated into complex kidney organoids. Generation of podocytes—the filtering cells of the kidney—in these organoids is of great interest, because podocytes are highly specialized cells that regenerate poorly in vivo and are challenging to culture using conventional methods. However, hPSC-podocytes differ from cultured podocytes in appearance and gene expression, and it is important to determine the developmental stage of hPSC-podocytes and their ability to recapitulate disease phenotypes. In this study, we address these questions by comparing hPSC-podocytes to developing podocytes in human and mouse kidneys. We demonstrate that hPSC-podocytes mimic developing podocytes in vivo at the capillary loop stage of glomerular maturation, both structurally and in disease phenotype, providing new insight into the genetic mechanisms of podocyte specialization. This establishes a powerful new tool for genetic studies of human podocyte development and disease.

### INTRODUCTION

Humans are born with a fixed number of kidney subunits, called nephrons. Progressive and irreversible reduction in nephron number causes end-stage renal disease, affecting two million people worldwide, in which kidney function fails, and either dialysis or kidney

transplant is required to sustain life. These treatments are of limited availability and efficacy, prompting interest in new therapeutic strategies based on the expansion of nephron progenitor cell populations that arise during kidney development [1–5], with the ultimate goal of generating new kidney tissues for transplantation [6–9].

<sup>a</sup>Division of Nephrology, <sup>b</sup>Kidney Research Institute, <sup>c</sup>Institute for Stem Cell and Regenerative Medicine, <sup>d</sup>Department of Medicine, <sup>i</sup>Division of Hematology, Department of Medicine, and <sup>k</sup>Department of Bioengineering, University of Washington School of Medicine, Seattle, Washington, USA; <sup>e</sup>The Biomedical Research Centre, <sup>f</sup>Department of Medical Genetics, and <sup>l</sup>Department of Cellular and Physiological Sciences, University of British Columbia, Vancouver, British Columbia, Canada; <sup>g</sup>Division of Nephrology, Vanderbilt University School of Medicine, Nashville, Tennessee, USA; <sup>h</sup>Department of Electrical Engineering and <sup>j</sup>Paul G. Allen School of Computer Science and Engineering, University of Washington, Seattle, Washington, USA

\*Contributed equally.

Correspondence: Kelly M. McNagny, Ph.D., The Biomedical Research Centre, University of British Columbia, Vancouver, British Columbia, Canada V6T 1Z3. Telephone: 1-604-822-7824; Fax: 1-604-822-7815; e-mail: kelly@brc.ubc.ca; or Benjamin S. Freedman, Ph.D., Division of Nephrology, Department of Medicine, University of Washington School of Medicine, 850 Republican St, Box 358056, Seattle, Washington 98109, USA. Telephone: 1-206-685-4653; Fax: 1-206-685-1357; e-mail: benof@uw.edu

Received February 16, 2017; accepted for publication September 4, 2017; first published online in *STEM CELLS EXPRESS* September 14, 2017.

<http://dx.doi.org/10.1002/stem.2707>

Human pluripotent stem cells, or hPSCs, are both self-renewing and pluripotent, providing a renewable source of diverse cells and tissues for laboratory studies and regeneration [10, 11]. hPSCs include both embryonic stem cells (ESCs) derived from embryos and induced pluripotent stem cells (iPSCs) reprogrammed from adult cells. Recently, multiple groups have published protocols describing the generation of kidney tissues from hPSCs [3–5]. In these protocols, hPSCs differentiate stepwise, first into primitive streak mesendoderm, subsequently into nephron progenitor cells expressing *sine oculis-related 2* (*SIX2*), and finally into organoids containing segments of distal tubules, proximal tubules, and podocytes [3–5, 12–14]. This provides a new resource for modeling human kidney disease and regeneration.

The generation of hPSC-derived podocytes (hPSC-podocytes) in these cultures is particularly interesting because primary podocytes are highly specialized, terminally differentiated epithelial cells that have been challenging to study in vitro or regenerate in vivo [15–17]. Mature podocytes have elaborate basal membrane extensions (foot processes), which are linked together by specialized junctions (slit diaphragms), and interdigitate around glomerular capillaries to form a sieve-like filter for the blood [18–20]. Failure to properly form or maintain these structures results in defective urine production, which can be fatal [21–23]. hPSC-podocytes express several markers associated with podocytes, such as WT1, podocalyxin, synaptopodin, and nephrin, suggesting that these cells may be useful for disease modeling experiments and possibly cell therapy [4, 5, 24].

To establish the validity of this new system and advance the field, it is important to determine the developmental stage of hPSC-podocytes and their ability to phenocopy genetic disease. Microarray datasets of purified hPSC-podocytes show significant overlap with published mouse and human datasets, but the top genes do not cluster clearly with kidney tissues [24]. The rounded, tightly clustered appearance of hPSC-podocytes also differs markedly from that of cultured podocytes, which adopt a flat, enlarged morphology with irregular edges [15]. hPSC-podocytes can form extensions from their basal plasma membranes, suggested to represent “primary” or “secondary” foot processes, but it is not clear whether they possess definitive, interdigitating, tertiary foot processes typical of mature podocytes in vivo [4, 13, 24]. Gene-edited hPSCs lacking podocalyxin (*PODXL*<sup>−/−</sup>) exhibit defects in junctional organization and podocyte adhesion, providing the first evidence that hPSC-podocytes have potential to model disease [5]. However, ultrastructural analysis of these hPSC-podocytes has not been performed, and the mechanisms underlying these defects and their relevance to podocyte development in vivo are not yet clear.

To address these gaps, we perform here a detailed, quantitative comparison of hPSC-podocytes with developing podocytes in vivo, including *PODXL*<sup>−/−</sup> mutants and mouse models. This work demonstrates that hPSC-podocytes resemble podocytes in vivo at the capillary loop stage (CLS) of glomerular development, and reveal a new role for podocalyxin-induced microvilli in this critical stage of differentiation.

## MATERIALS AND METHODS

### Kidney Organoid Differentiation and Fixation

Cell lines included WA09 ESCs (WiCell, Madison, WI, <http://www.wicell.org>; female), WTC11 iPSCs (Gladstone Institute;

male), and *NPHS1-GFP* 201B7 iPSCs (Kumamoto University; female). Passages used were between 30 and 60. Kidney organoid differentiation was performed as described previously [5]. hPSCs were plated at a density of 45,000 cells per well in mTeSR1 (STEMCELL Technologies, Vancouver, Canada, <http://www.stemcell.com>) + 10  $\mu$ M Y27632 (LC Laboratories, Woburn, MA, <http://www.lclabs.com>) on glass plates (LabTek) coated with 3% GelTrex (ThermoFisher Scientific) (day −3), which was changed to 1.5% GelTrex in mTeSR1 (day −2), mTeSR1 (day −1), RPMI (ThermoFisher Scientific, Waltham, MA, <http://www.thermofisher.com>) + 12  $\mu$ M CHIR99021 (Tocris, Bristol, UK, <http://www.tocris.com>) (day 0), RPMI + B27 supplement (ThermoFisher Scientific) (day 1.5), and fed every 2–3 days to promote kidney organoid differentiation. Organoids were fixed on day 18, unless otherwise noted. To fix, an equal volume of phosphate-buffered saline (PBS) (ThermoFisher Scientific) + 8% paraformaldehyde (Electron Microscopy Sciences, Hatfield, PA, <http://www.emsdiasum.com>) was added to the media for 15 minutes, and the sample was subsequently washed three times with PBS. Kidneys (days 60–120) were obtained from the Laboratory of Developmental Biology (University of Washington) with informed consent and approval of the institutional review board. To generate cryosections, halved kidneys were fixed in PBS + 4% paraformaldehyde for 1 hour, incubated overnight in 30% sucrose (Sigma, St. Louis, MO, <http://www.sigmaldrich.com>) in water, mounted in Tissue-Tek (Sakura, Torrance, CA, <http://www.sakuraus.com>), and flash frozen with liquid nitrogen. For paraffin sections, tissues were fixed overnight with methacarn: 60% absolute methanol, 30% chloroform, 10% glacial acetic acid (Sigma), and subsequently paraffin-embedded. Paraffin tissue sections were deparaffinized with three 2-minute washes in xylene, followed by 100%, 85%, and 70% ethanol, and heated in citrate buffer pH 6.0 (Sigma) in a pressure cooker (Instant Pot IPDUO60, Amazon, Seattle, WA, <http://www.amazon.com>) for 3 minutes before immunostaining.

### Immunofluorescence

For immunofluorescence, fixed organoid cultures or tissue sections were blocked in 5% donkey serum (Millipore, Billerica, MA, <http://www.emdmillipore.com>) + 0.3% Triton-X-100/PBS, incubated overnight in 3% bovine serum albumin (Sigma) + PBS with primary antibodies, washed, incubated with Alexa-Fluor secondary antibodies (ThermoFisher Scientific), washed, and stained with 4',6-diamidino-2-phenylindole or mounted in Vectashield H-1000. Labels included fluorescent-labeled *Lotus tetragonolobus* lectin (LTL) (Vector Labs, Burlingame, CA, <http://www.vectorlabs.com>, FL-1321, 1:500 dilution) and primary antibodies targeting ZO-1 (ThermoFisher Scientific 339100, 1:100), hPODXL (R&D, Minneapolis, MN, <http://www.rndsystems.com>, AF1658, 1:500), SYNPO (Santa Cruz, Dallas, TX, <http://www.scbt.com>, sc-21537, 1:100), NPHS1 (R&D AF4269, 1:500), NPHS2 (Abcam, Cambridge, UK, <http://www.abcam.com>, ab50339, 1:300), PAX2 (Abnova, Taiwan, <http://www.abnova.com> H00005076-M01, 1:100), PAX8 (Proteintech, Rosemont, IL, <http://www.ptglab.com>, 10336-1-AP, 1:300), and WT1 (Santa Cruz sc-192, 1:100). For PAX2, PAX8, and WT1, paraffin sections were used to determine localization patterns in vivo. Some cytoplasmic staining of these transcription factors was also observed, which was likely an artifact. Antibodies for PAX2 and PAX8 may show some

cross-reactivity. Images are representative of stainings from three or more separate experiments.

### Electron Microscopy

Kidney organoid cultures were fixed in PBS + 4% paraformaldehyde for 5 minutes, collected by scraping, pelleted at 300g, and resuspended in EM fix: 0.15 M sodium cacodylate trihydrate (Sigma) dissolved in water (pH 7.3) containing 4% formaldehyde and 2% glutaraldehyde (Electron Microscopy Sciences). Kidney tissues (1 mm diameter) were placed directly into electron microscopy (EM) fix. Samples were post-fixed with osmium tetroxide solution (Sigma), dehydrated in serial ethanol dilutions (Sigma), and embedded in epoxy resin. Ultrathin sections (80 nm) were mounted on 200 mesh copper grids, stained with uranyl acetate and lead citrate (Electron Microscopy Sciences), and imaged with JEOL JEM-1010 and FEI Tecnai G2 Spirit transmission electron microscope (TEM). Images were representative of at least two kidneys containing numerous glomeruli per condition.

### Image Quantification and Statistical Analysis

Line scans of equivalent length were drawn basal to apical through representative cells and the raw fluorescence intensity values were averaged for each point along the line scan. For TEM images, microvillus density was measured for cells that had a clear apico-lateral surface by counting microvilli along this surface and dividing by its perimeter, without analyzing the basement membrane or foot processes. Cell separation was measured between two cell bodies that were directly adjacent to each other with nothing in-between by drawing a line between their two lateral membranes at a site of approximately median separation between the two cells' midlines. Foot processes were defined as continuous membrane events proximal to the glomerular basement membrane (GBM) on the side of the Bowman's space, which were separated by a slit diaphragm. The number of foot processes was counted and normalized to the length of the adjacent GBM. Statistical analysis was performed using a two-tailed *t* test for samples with unequal variance (heteroscedastic) between the wild-type and mutant cohorts.

### Generation of Podocalyxin Mutants

Gene-edited *PODXL*<sup>-/-</sup> hPSCs and isogenic control lines were generated from WA09 hESCs [5]. Strains were backcrossed onto a C57Bl/6 background for at least eight generations (F8). Germ-line *Podxl*-null mice (*Podxl*<sup>-/-</sup>) and wild type (WT) (+/+) control embryos were generated by intercrossing *Podxl*<sup>+/-</sup> mice [21]. The "floxed" *Podxl* mouse strain (*Podxl*<sup>fl/fl</sup>) was generated as described [25]. For the *Podxl.Cdh5Cre* strain, *Podxl*<sup>fl/+</sup>*Cre*<sup>+/+</sup> sires were crossed with *Podxl*<sup>fl/fl</sup>*Cre*<sup>+/+</sup> dams to generate pups with *Podxl*<sup>fl/fl</sup>*Cre*<sup>+/+</sup> ("Het") or *Podxl*<sup>fl/+</sup>*Cre*<sup>+/+</sup> genotypes ("KO"). For the *Podxl.TekCre* strain, *Podxl*<sup>fl/fl</sup>*Cre*<sup>+/-</sup> sires were crossed with *Podxl*<sup>+/-</sup>*Cre*<sup>-/-</sup> dams to generate pups with the following genotypes: *Podxl*<sup>fl/+</sup>*Cre*<sup>+/-</sup> ("Het"), *Podxl*<sup>fl/-</sup>*Cre*<sup>+/-</sup> ("KO"), *Podxl*<sup>fl/+</sup>*Cre*<sup>-/-</sup> ("WT"), and *Podxl*<sup>fl/-</sup>*Cre*<sup>-/-</sup> ("WT"). Experiments using strains with conditional "floxed" alleles were performed using mice with Cre+ genotypes only (i.e., "Het" and "KO" genotypes) to control for potential Cre-expression effects.

### Optical Tweezers

Confluent hPSCs in a 35-mm dish were washed briefly with PBS and then cultured in Versene for 6 minutes and 30 seconds in the incubator, which was carefully aspirated from the edge of the well

without detaching cells. One milliliter of mTeSR1 + 10 μM Y27632 was added, triturated to detach cells, passed through a 40-μm filter, counted, and diluted to 2.3 × 10<sup>4</sup> cells per milliliter in 3 ml mTeSR1 + 6 μM Y27632 + 20 μl HEPES, and cells were transported on wet ice to the optical tweezers setup. Cells in solution were added into a 60-mm sterilized petri dish under an AXIO Imager D1m microscope (Zeiss, Oberkochen, Germany, <http://www.zeiss.com>). A 1064 nm Nd:YVO<sub>4</sub> near-infrared laser and 50X objective lens (N.A. = 0.55) were used to manipulate pairs of cells to the middle of the dish by optical tweezers, to avoid cell adhesion to the chamber surface. The pair of cells was placed as close as ~5 μm [26]. The laser was aimed in-between the two cells and activated at an intensity of 0.67 mW/μm<sup>2</sup> to attract them inwards. The distance between the two cells was measured when motion ceased. Experiments in which the cells became stuck to each other or to the chamber surface were excluded from the analysis.

### RNA Sequencing and Analysis

RNA was prepared from isogenic sets of hPSCs using the RNEasy Mini Kit (Qiagen, Hilden, Germany, <http://www.qiagen.com>), checked for high integrity on an Agilent Bioanalyzer, and prepared using the TruSeq stranded mRNA library kit (Illumina, San Diego, CA, <http://www.illumina.com>). Samples were sequenced on an Illumina NextSeq500 75 × 75 paired end high output run and aligned to hg19 reference sequence. DESeq was used for differential gene expression analysis [27]. Two models were built. The null model assumed gene expression variation was purely due to experimental batches; the full model included mutant versus control as an additional predictor. A gene was identified as significant when the full model fit was better (Benjamini-Hochberg FDR < 0.1). topGO R package was used for Gene Ontology enrichment analysis [28]. Ingenuity Pathway Analysis (Qiagen) was used to identify top upstream regulators. RNA-seq samples were deposited in the Gene Expression Omnibus (NCBI) under accession number (GSE103547).

### Electrostatic Force Calculation

Distance between cells "*N*" and cell radius "*r*" were calculated empirically by averaging TEM measurements. The isoelectric point (pI) of human podocalyxin was approximated by summing the logarithmic acid dissociation constant (pKa) values of the residues of the primary sequence. The number of sialic acids per podocalyxin molecule was estimated based on the literature [29]. Electrostatic force generated by podocalyxin was calculated assuming direct interference between perfectly opposite microvilli with 10 podocalyxin molecules per microvillus and did not include electrostatic contribution from neighboring microvilli which would account for a small increase in force (~10% in two dimensions). As different microvillus arrangements and neighboring charges would increase electrostatic interference, our force calculation is likely to be an underestimate. Application of Gauss' law yielded the same value as Coulomb's law.

## RESULTS

### hPSC-Podocytes Express Markers of CLS Podocytes

We used an adherent culture protocol to differentiate hPSCs into kidney organoids [5], in which proximal tubules and hPSC-podocytes could be distinguished using LTL and podocalyxin, respectively (Fig. 1A; Supporting Information Fig. S1A, S1B).

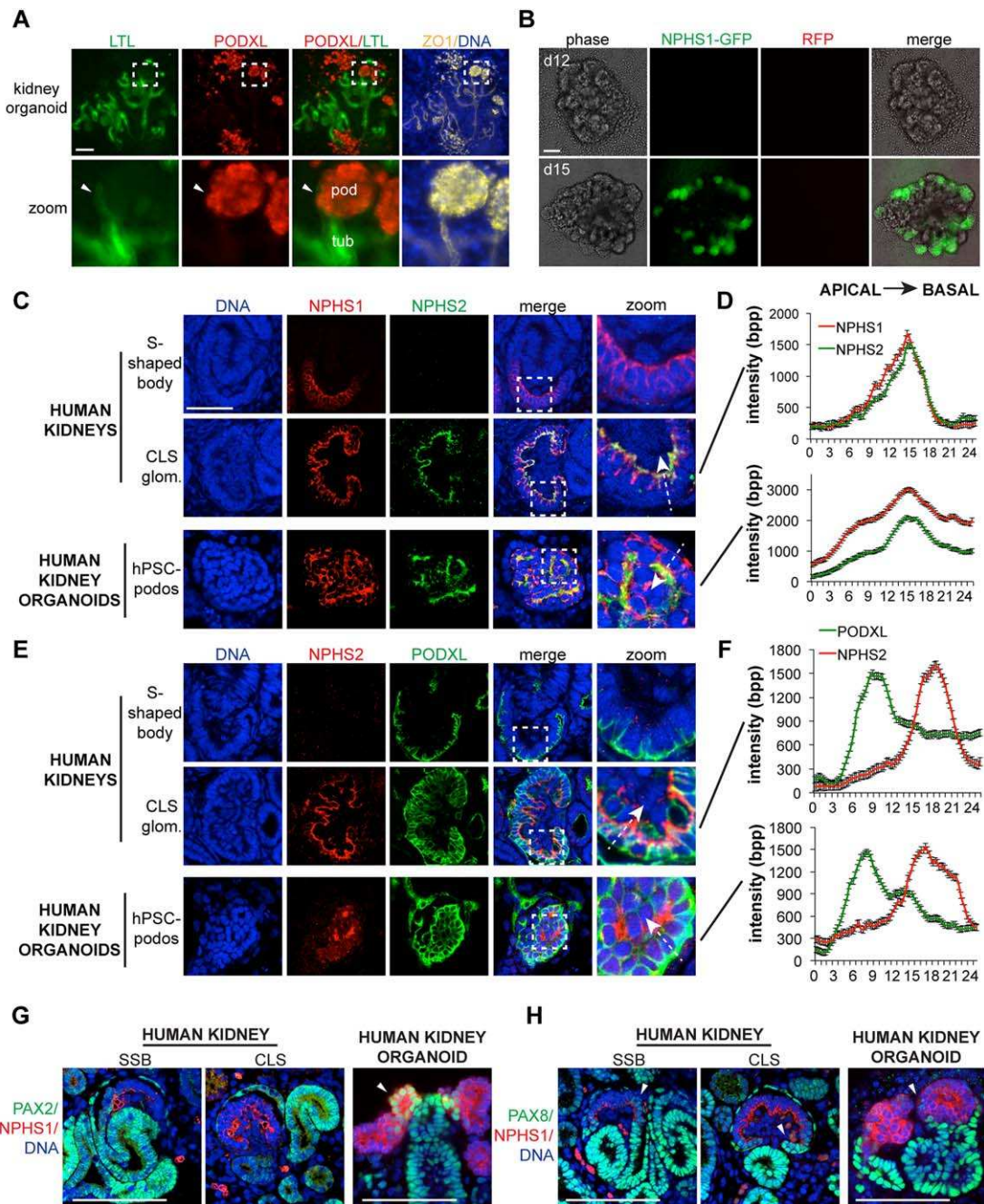


**Figure 1.** Marker localization in human pluripotent stem cell-podocytes and capillary loop stage podocytes. **(A):** Representative wide-field fluorescence image of kidney organoids showing tubule (*Lotus tetragonolobus* lectin) and podocyte (podocalyxin [PODXL]) populations co-localized with the tight junction protein ZO-1. Zoom shows dashed white-boxed region where a tubule forms a junction with a cluster of podocytes. Arrowhead indicates tubule-like cells bordering the podocyte cluster. **(B):** NPHS1-GFP organoids on days 12 and 15 of differentiation. Red channel is included as a negative control for autofluorescence. **(C):** Representative confocal optical sections and **(D)** averaged raw fluorescence intensities in line scans drawn through podocytes, showing co-localization of podocin (NPHS2) with nephrin (NPHS1) or **(E, F)** with PODXL in human glomeruli and kidney organoids. Zoom of boxed regions are shown at right for the merged images. White-dashed arrows demonstrate how line scans were drawn. Line scans are 24  $\mu\text{m}$  through individual cells ( $n = 10$ ,  $\pm$ SEM). **(G):** Representative confocal images of kidney tissues (left) or human kidney organoids (right) showing co-localization of nephrin with antibodies raised against PAX2 and **(H)** PAX8. Arrowheads indicate PAX2 or PAX8 co-localization with nephrin at the edge of the podocyte cluster. Scale bars = 100  $\mu\text{m}$ . Abbreviations: bpp, bits per pixel (raw intensities); CLS, capillary loop stage; GFP, green fluorescent protein; hPSC, human pluripotent stem cell; Podo, podocytes; RFP, red fluorescent protein; SSB, S-shaped body; Tub, tubules.

Tubule-like cells bordering and encapsulating podocyte clusters did not express podocalyxin, but also exhibited weaker LTL binding affinity compared with the proximal tubule (Fig. 1A). Time course analyses confirmed that tubules and podocytes arose from

aggregates of SIX2<sup>+</sup> nephron progenitor cells after 2–3 weeks in culture, concomitant with an upregulation of WT1, consistent with our previous characterization of this differentiation pathway (Supporting Information Fig. S1C, S1D). In lineage reporter hPSCs

[24], green fluorescent protein (GFP) was expressed from the nephrin (*NPHS1*) locus in hPSC-podocytes (Fig. 1B).

To determine the developmental stage of hPSC-podocytes, we directly compared gene expression and localization between kidney organoids *in vitro* and kidney organs. During organogenesis, podocytes first become detectable in primitive nephrons called S-shaped bodies (SSBs), and subsequently mature in CLS glomeruli [18]. We identified SSBs and CLS glomeruli in tissue sections from human kidneys and assessed these for expression and localization of nephrin and podocin (*NPHS2*), components of the slit diaphragm [22, 23]. Nephrin was expressed in podocytes of both SSBs and CLS glomeruli, whereas podocin was restricted to CLS glomeruli (Fig. 1C). Both proteins strongly co-localized at the GBM and were absent in neighboring tubular cells (Fig. 1C, 1D). In kidney organoids, nephrin and podocin were enriched in linear, basement membrane-like tracks at the basal side of hPSC-podocytes (Fig. 1C). Quantification of intensity peaks for nephrin and podocin revealed that they overlapped in hPSC-podocytes, similar to their patterns *in vivo* in CLS podocytes (Fig. 1D).

Podocalyxin is a heavily sialylated member of the CD34 protein family that is highly expressed in podocytes *in vivo* and in hPSC-podocytes [5, 21, 29]. In primary tissue sections from SSBs and CLS glomeruli, podocalyxin localized exclusively to the apical surface of podocytes, contrasting with the basement membrane localization of nephrin and podocin (Fig. 1E). Similarly, in kidney organoids, podocalyxin localized to the apical cell surface of hPSC-podocytes (Fig. 1E). In both hPSC-podocytes and CLS podocytes, the intensity peaks of podocalyxin and podocin did not overlap and were found on opposite sides of the cell (Fig. 1F).

The transcription factors paired box 2 (*PAX2*) and *PAX8* are downregulated during podocyte specification, whereas *WT1* is upregulated and linked to nephrin expression [30–33]. Previously, in RT-PCR analyses of whole kidney organoid cultures, *PAX2* and *WT1* were found to be co-expressed, raising the question of whether *PAX* genes were appropriately downregulated in hPSC-podocytes [5]. To distinguish between tubular and podocyte *PAX* gene expression, we performed immunofluorescence analysis. In both SSBs and CLS glomeruli, *PAX2* and *PAX8* exhibited similar staining patterns, with bright nuclear immunofluorescence in tubules (Fig. 1G, 1H). *PAX2* and *PAX8* immunofluorescence was absent in the nuclei of nephrin<sup>+</sup> podocytes at both stages, although co-localization with nephrin was occasionally observed at the outer edges of podocyte clusters, where they bordered tubules (Fig. 1G, 1H). Similarly, in kidney organoids, tubular cells expressed *PAX2* and *PAX8* in nuclei, while neighboring hPSC-podocytes downregulated these genes except where bordering tubules (Fig. 1G, 1H). Thus, sustained expression of *PAX* genes in whole organoid cultures reflected upregulation by tubular cells, not hPSC-podocytes. Conversely, *WT1* was specifically expressed in the nuclei of nephrin<sup>+</sup> cells in both human kidneys and human kidney organoids (Fig. 2A, 2B; Supporting Information Fig. S1D). Nephrin and *WT1* were specific to the podocytes in organoids and were not expressed in neighboring tubules (Fig. 2B). Collectively, these data indicated that marker expression and localization in hPSC-podocytes resembles CLS podocytes *in vivo*.

### Junctions Migrate Basally in hPSC-Podocytes

An unusual feature of podocyte maturation is the migration of tight junction components, such as ZO-1, from the apical

to the basement membrane [18–20]. We first confirmed this localization pattern in human kidneys. In SSBs, immature podocytes could be identified based on their low, but detectable, co-expression of nephrin and *WT1* (Fig. 2A). ZO-1 localized to the sub-apical plasma membrane of these cells, similar to its expression in the tubule (Fig. 2A). In CLS glomeruli, however, ZO-1 localization switched from the apical to the basement membrane (Fig. 2A; Supporting Information Fig. S2A). Line scan quantification confirmed this relocation of the ZO-1 intensity peak from apical to basal, with an average migrational distance of approximately 10  $\mu\text{m}$  (Fig. 2A).

In kidney organoids, we identified a population of columnar, *WT1*-positive, polarized epithelial cells with low but detectable nephrin expression (nephrin<sup>lo</sup> *WT1*<sup>+</sup> *ZO1*<sup>+</sup>) that formed a continuous epithelium with clusters of hPSC-podocytes expressing the same markers with higher nephrin levels (Fig. 2B). Along this linear continuum, ZO-1 localization gradually migrated from the apical surface of nephrin<sup>lo</sup> cells to the basal surface of nephrin<sup>hi</sup> cells (Fig. 2B; Supporting Information Fig. S2B). Basal localization of ZO-1 was strongly enriched within the nephrin<sup>hi</sup> portion of the epithelium, corresponding to a rounded rather than columnar epithelial morphology (Fig. 2B; Supporting Information Fig. S2B). Line scan analysis revealed the overall migrational distance of ZO-1 to be approximately 12  $\mu\text{m}$  within this epithelium (Fig. 2B). We further examined junctional organization during the time course of podocyte differentiation. Young hPSC-podocytes (day 11 of differentiation) formed epithelial layers one single cell in thickness, with a characteristic ellipsoid morphology. ZO-1 localized to lateral and sub-apical foci in these cells, whereas the slit diaphragm marker synaptopodin (*SYNPO*) was enriched at the basement membrane (Supporting Information Fig. S2C). At later time points (day 18 and onwards), podocytes formed paired layers whose basement membranes were connected by zipper-like tracks containing both synaptopodin and ZO-1 (Supporting Information Fig. S2C). These findings suggested that apical-to-basal migration of ZO-1 is recapitulated during the maturation of hPSC-podocytes *in vitro*, resulting in their self-organization into conjoined layers at later stages of differentiation.

### Ultrastructure of hPSC-Podocytes in Kidney Organoids

We further analyzed these structures by TEM to determine their cellular ultrastructure at day 18, a time point at which hPSC-podocytes adopted a mature appearance by immunofluorescence. In organoid cultures, tubular cells exhibited a columnar morphology and made direct contacts along their lateral plasma membranes to form a smooth-edged epithelium (Fig. 3A). Tight junctions formed between these cells at their sub-apical surface, adjacent to the tubular lumen (Fig. 3A). In contrast to the columnar morphology of the tubules, hPSC-podocytes formed clustered aggregates of rounded cells containing prominent nuclei with scant cytoplasm, and were readily detected by their distinct morphology (Fig. 3A).

Within these aggregates, hPSC-podocytes were arranged intermittently along basement membrane-like tracks (Fig. 3A). Neighboring hPSC-podocytes did not form close contacts between their lateral plasma membranes. Rather, numerous microvilli projected outwards from the lateral membranes, filling the spaces between cells (Fig. 3A). A stalk-like cell body containing mitochondrial cristae and organelles connected each cell to the basement membrane, where junction-like structures were observed at points of cell-cell contact (Fig. 3A). Basal to these

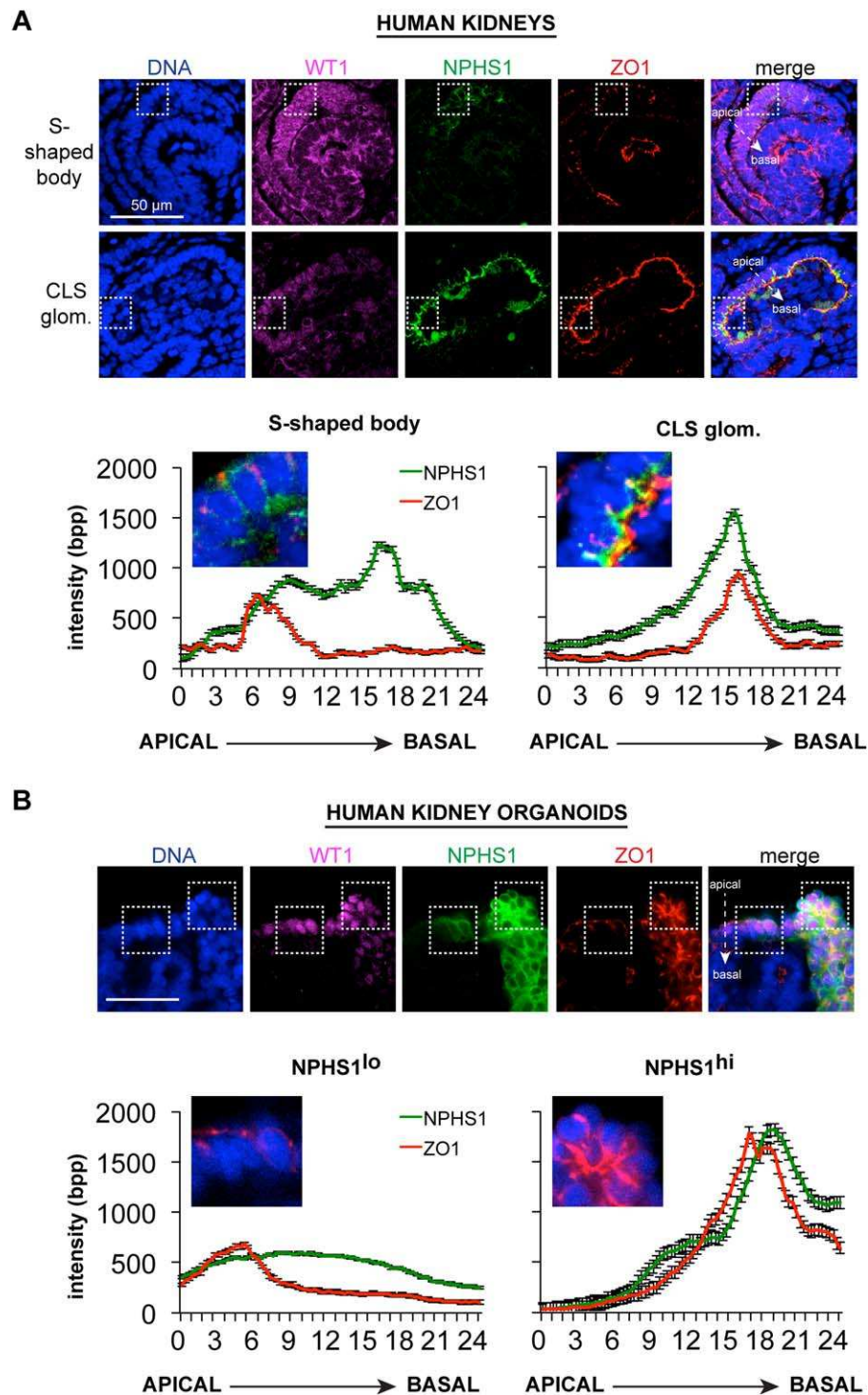


**Figure 2.** Junctions migrate basally during maturation of human pluripotent stem cell-podocytes and capillary loop stage podocytes. **(A):** Representative confocal optical sections (top) and averaged raw fluorescence intensity line scans (bottom) showing ZO-1 and NPHS1 localization in developing human kidneys and **(B)** human kidney organoids. Zoom of boxed regions without WT1 channel (human kidneys), or without WT1 and nephrin (human kidney organoids), are shown below images. Apical and basal sides of the epithelium are labeled in merged images. White-dashed arrows demonstrate how line scans were drawn. Line scans are 24  $\mu\text{m}$  through individual cells ( $n = 10$ ,  $\pm$ SEM).  $y$ -axes are the same throughout. Scale bars = 20  $\mu\text{m}$ . Abbreviations: CLS, capillary loop stage; NPHS1, nephrotic syndrome 1 (nephrin).

junctions, hPSC-podocytes extended membranous processes, but robust interdigitating foot processes were not observed (Supporting Information Fig. S3A).

These findings were compared with TEM of human kidneys. As podocytes matured into CLS glomeruli, microvilli

appeared between them in intercellular spaces (Fig. 3B). CLS podocytes bore a striking resemblance to hPSC-podocytes, with apical nuclei, apical and lateral microvilli, scant cytoplasm, and a common basement membrane (Fig. 3A, 3B). Similar cellular architectures were also observed in prenatal mouse

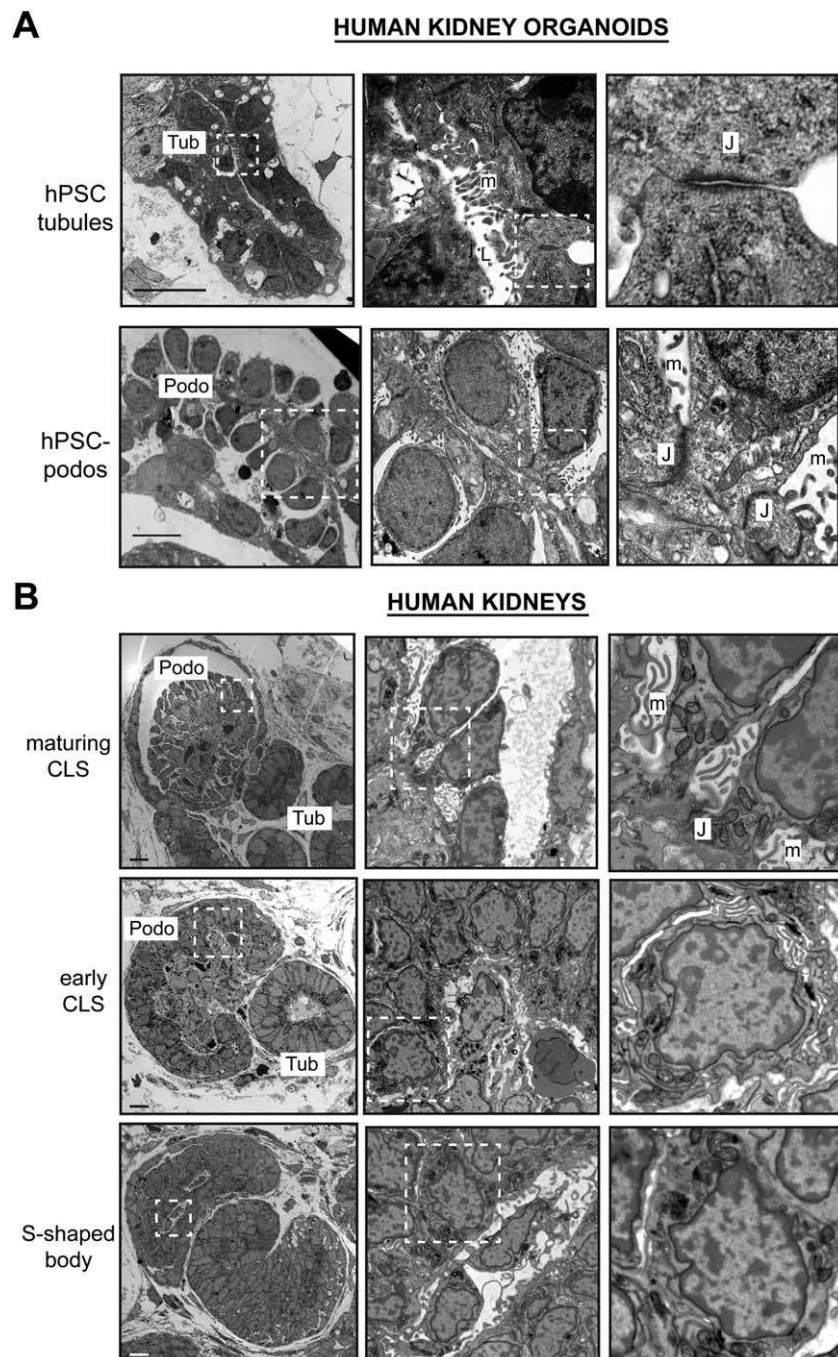


**Figure 3.** The ultrastructure of human pluripotent stem cell (hPSC)-podocytes resembles capillary loop stage (CLS) podocytes in vivo. **(A):** Representative transmission electron microscopic images of tubules and podocytes in human kidney organoids. Arrows indicate tubule-like cells bordering the podocyte aggregate. **(B):** Developing glomeruli at different stages in human kidneys. Note similarity between maturing CLS podocytes and hPSC-podocytes at highest magnification. Scale bars = 10  $\mu$ m. Abbreviations: CLS, capillary loop stage; hPSC, human pluripotent stem cell; J, junctions; L, lumen; m, microvilli; Podo, podocytes; Tub, tubules.

kidneys, which contained immature glomeruli (Supporting Information Fig. S3B). In contrast to these, podocytes from adult mice exhibited distinctive, interdigitating foot processes and slit diaphragms (Supporting Information Fig. S3C).

#### Podocalyxin Regulates Microvillus Formation and Cell Spacing in Podocytes

To complement descriptive studies, we investigated whether hPSC-podocytes could provide new insights into the genetic

mechanisms of CLS podocyte maturation. We therefore performed ultrastructural analysis on hPSC-podocytes derived from *PODXL*<sup>-/-</sup> hPSCs, which exhibit defects in junctional organization by confocal microscopy but have not previously been examined with TEM [5]. Surprisingly, ultrastructural analyses using TEM revealed that *PODXL*<sup>-/-</sup> hPSC-podocytes exhibited a near-total lack of microvilli, compared with non-mutant controls (Fig. 4A). This reduction in microvilli was accompanied by a reduction in the lateral spaces between adjacent *PODXL*<sup>-/-</sup> hPSC-podocytes,



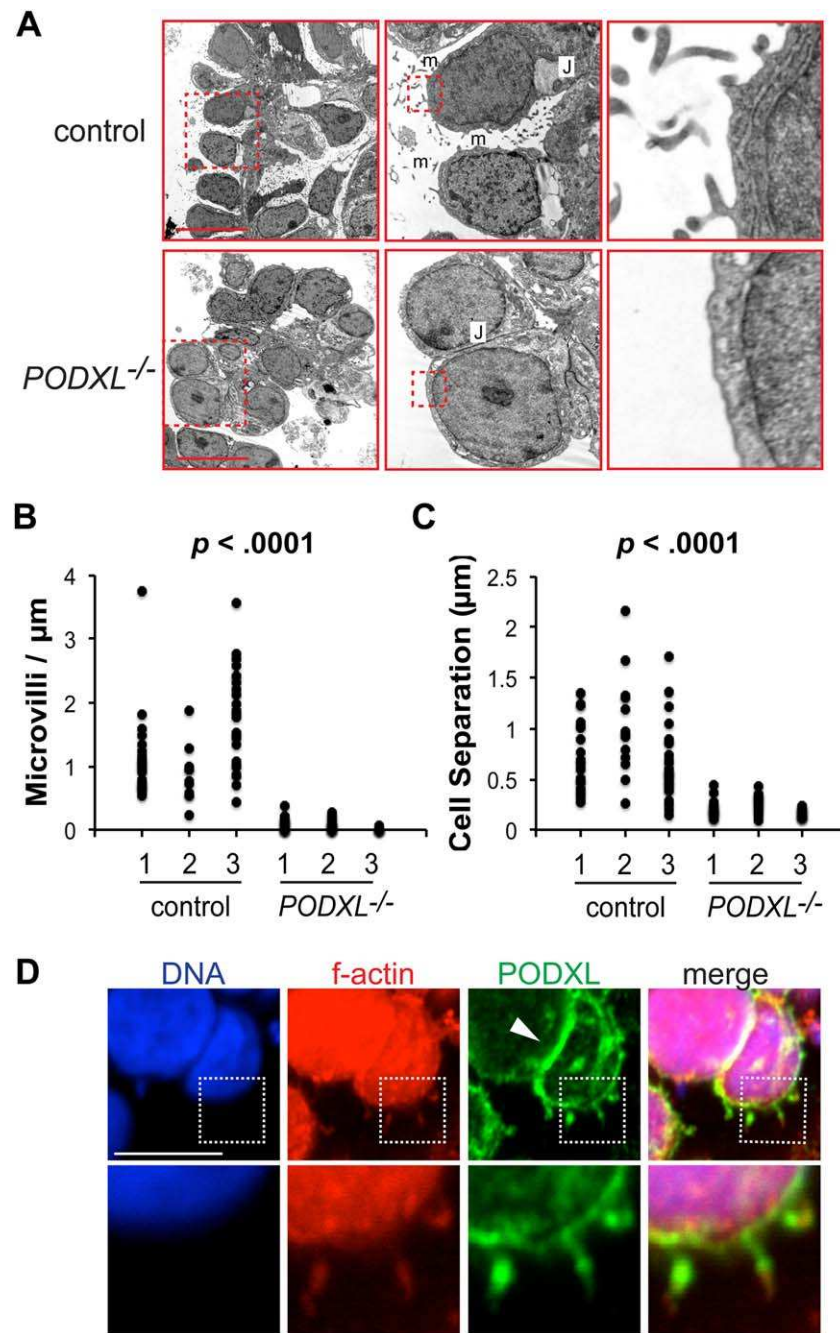


**Figure 4.** Podocalyxin regulates microvillus formation and cell spacing in human pluripotent stem cell (hPSC)-podocytes. **(A):** Representative transmission electron microscopic (TEM) images of control and *PODXL*<sup>-/-</sup> hPSC-podocytes. Progressive zooms are shown for boxed regions in TEM images. **(B):** Counts of microvillus number in *PODXL*<sup>-/-</sup> hPSC-podocytes, compared with non-mutant controls. Each point represents a single podocyte ( $n = 3$  experiments). **(C):** Quantification of separation distance between cell lateral membranes in these hPSC-podocytes, with associated  $p$  values. **(D):** Confocal section showing podocalyxin co-localization with filamentous actin at high magnification. Arrowhead highlights podocalyxin concentration between adjacent hPSC-podocytes. Boxed area is shown in zoom and highlights microvilli. Scale bars = 10  $\mu\text{m}$ . Abbreviations: J, junctions; m, microvilli.

and, correspondingly, an increase in the formation of lateral cell–cell junctions, which were rarely observed in control hPSC-podocytes of identical genetic background (Fig. 4A). Quantification of these phenotypes revealed the changes in microvillus number and lateral cell-to-cell distance to be approximately 10-fold and fivefold in magnitude, respectively (Fig. 4B, 4C). Confocal imaging of hPSC-podocytes further revealed that apical microvilli in hPSC-podocytes contained podocalyxin (Fig. 4D).

Our observation that podocalyxin was required for podocyte microvillus formation was a novel finding, which was not previously described in podocalyxin-deficient (*Podxl*<sup>-/-</sup>) mice [21]. To validate hPSC-podocytes as a genetic model of CLS development, it was therefore important to determine whether this phenotype observed in human podocytes in vitro was also true of CLS podocytes in vivo. To investigate the role of podocalyxin in vivo, we generated new *Podxl*<sup>-/-</sup>

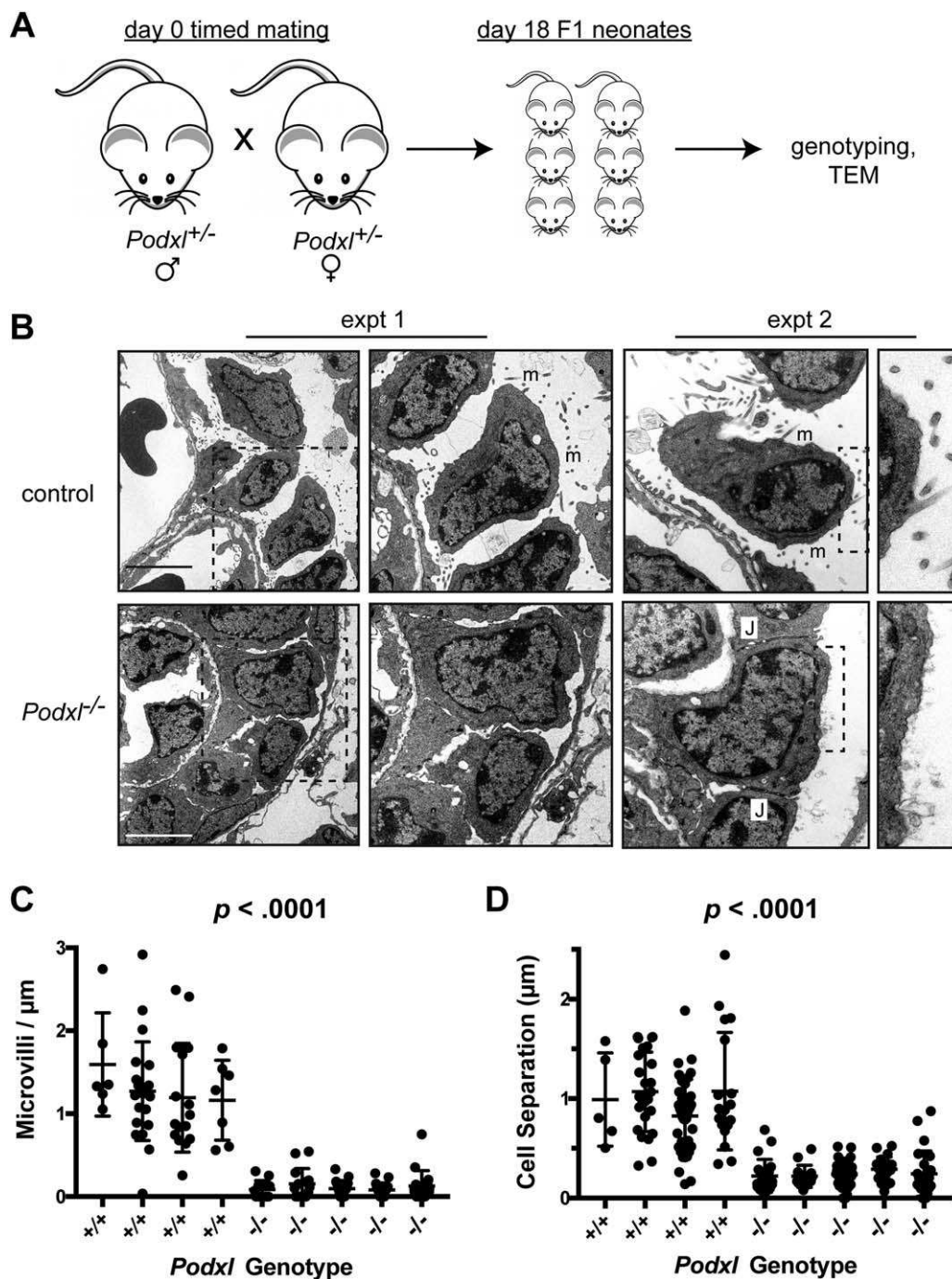


**Figure 5.** Podocalyxin regulates microvillus formation and cell spacing in mouse podocytes. **(A):** Schematic representation of knockout mouse generation and analysis. **(B):** Transmission electron microscopic images of podocytes from *Podxl*<sup>-/-</sup> prenatal mice (E18.5) or age-matched littermate controls. Images from two representative littermate experiments are shown. Zoom is shown to the right for dashed boxed regions. **(C):** Quantification of microvillus number and **(D)** cell separation in *Podxl*<sup>-/-</sup> podocytes and littermate controls, with associated *p* values. Each point represents a single podocyte ( $n = 4$  control and 5 *Podxl*<sup>-/-</sup> mice,  $\pm$ SD). Scale bars = 5  $\mu\text{m}$ . Abbreviation: J, junctions; m, microvilli; TEM, transmission electron microscopy.

mice and analyzed microvillus formation in the glomeruli of these animals. As *Podxl*<sup>-/-</sup> mice die of anuria shortly after birth [21], prenatal mice (E18.5) were examined (Fig. 5A). TEM analyses of glomeruli in *Podxl*<sup>-/-</sup> mice showed a drastic decrease in the ability of podocytes to form microvilli, compared with littermate controls (Fig. 5B, 5C). Spacing between adjacent *Podxl*<sup>-/-</sup> podocytes was likewise greatly decreased (Fig. 5B, 5D). *Podxl*<sup>-/-</sup> mouse podocytes in vivo therefore

phenocopied *PODXL*<sup>-/-</sup> hPSC-podocytes in vitro, demonstrating that hPSC podocytes could reveal genetic mechanisms of CLS maturation.

In addition to podocytes, podocalyxin is also expressed in endothelial cells (ECs), where it can affect vascular permeability [25, 34]. To determine the effect of podocalyxin on glomerular ECs, we generated mice lacking podocalyxin specifically in the vasculature. Using two different lineage reporters, these

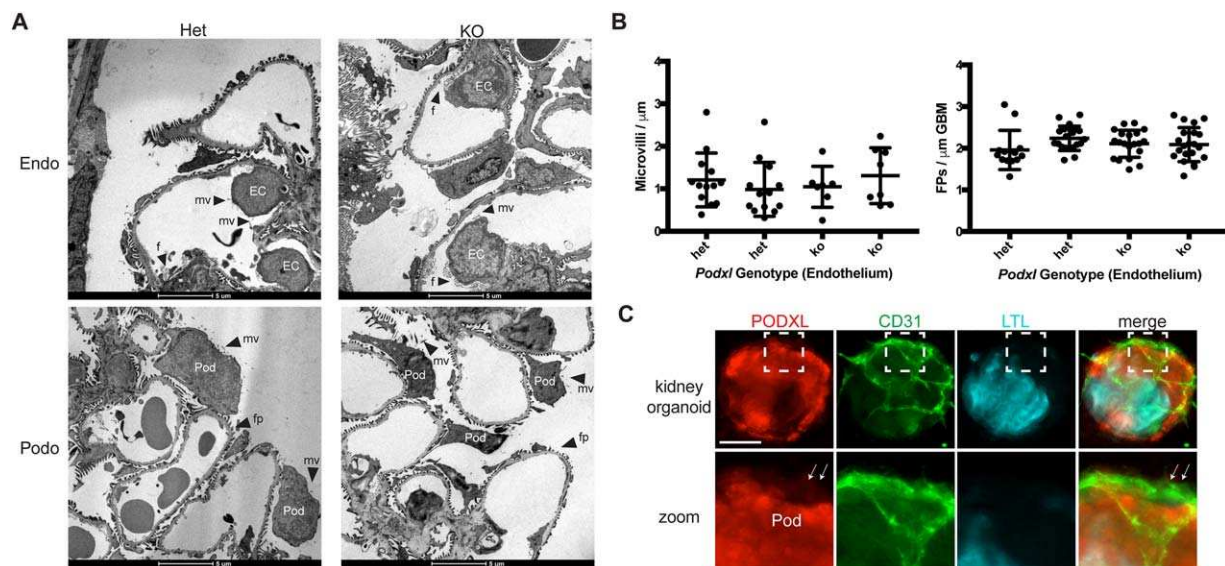


**Figure 6.** Loss of podocalyxin from endothelial cells does not significantly affect the morphology of glomerular endothelial cells or podocytes. **(A):** Transmission electron micrographs of glomerular endothelial cells (Endo) and podocytes (Podo) in *Cdh5*-driven podocalyxin knockout mice compared with controls. **(B):** Quantification of microvillus formation (microvilli per unit length of apico-lateral membrane) and foot process frequency (continuous membrane events separated by a slit diaphragm per unit length of basement membrane) in podocytes from *Cdh5-Cre* mice. Error bars, mean  $\pm$  SD. **(C):** Representative wide-field immunofluorescence images of podocalyxin expression in kidney organoids containing endothelial cells (CD31) and proximal tubules (*Lotus tetragonolobus* lectin). Zoom shows close-up of white-dashed boxed region. Arrows indicated faint podocalyxin staining in endothelial cells, relative to the underlying layer of podocytes. Scale bars = 5  $\mu\text{m}$  (A) or 100  $\mu\text{m}$  (C). Abbreviations: EC, endothelial cell; f, Fenestrae; fp, foot process; FPs, foot processes; GBM, glomerular basement membrane; KO, knockout; mv, microvillus; Pod, podocyte.

mice were healthy and viable with no obvious phenotype unless vascular leak was induced [25]. We detected no difference in the morphology of glomerular ECs or podocytes by TEM (Fig. 6A; Supporting Information Fig. S4A, S4B). Quantitative analysis revealed no differences in podocyte microvillus or foot process formation (Fig. 6B; Supporting Information Fig. S4C, S4D). In human kidney organoids, hPSC-podocytes were not identified solely on the basis of podocalyxin expression, but rather as tightly clustered, rounded cells that co-expressed synaptopodin, nephrin, podocin, and podocalyxin, at much higher levels than any other cells in the organoid or surrounding cells in the culture. hPSC-derived ECs also arose within kidney organoid cultures, as reported previously, but could be readily distinguished from hPSC-podocytes based on the expression of specific markers such as CD31, and by their chain-like networks, which extended beyond the organoid into the surrounding stroma [5]. Podocalyxin expression in hPSC-ECs was dramatically lower than in neighboring hPSC-podocytes, consistent with our previous report (Fig. 6C) [5]. Collectively, these data suggested that the kidney defects we observed in podocalyxin mutants were due to podocalyxin loss in podocytes, rather than in ECs.

The finding that podocalyxin induced microvillus formation, and localized to these microvilli, suggested that it might promote cell separation by establishing an anti-adhesive surface. To test this, we performed experiments using optical tweezers [26]. As hPSC-podocytes are terminally differentiated cells that cannot be readily purified or expanded, these experiments were performed on undifferentiated hPSCs, which strongly express podocalyxin. Control or *PODXL*<sup>-/-</sup> hPSCs were first dissociated to disrupt cell junctions, and were subsequently trapped in pairs using a laser to determine their minimum

separation distance (Fig. 7A). Under controlled laser power, *PODXL*<sup>-/-</sup> hPSCs consistently exhibited cell separation distances  $\sim$ 50% lower than control hPSCs (Fig. 7B). As this anti-adhesive effect occurred within a time frame of seconds and in the absence of pre-formed junctions, it suggested that steric or electrostatic alterations in membrane surface composition were responsible.

We further performed global gene analysis (RNA-Seq) to identify differentially expressed genes and pathways in *PODXL*<sup>-/-</sup> and control hPSCs. The top gene ontology terms enriched in *PODXL*<sup>-/-</sup> hPSCs were related to positive regulation of cell-cell adhesion (Fig. 7C). Podocalyxin itself was among the top differentially expressed genes (Fig. 7D). In addition to podocalyxin itself, this analysis suggested the possible involvement of additional factors, including ZFP28 and OLIG2, and upstream regulators, such as HNF1A and OTX2, not previously associated with podocalyxin (Fig. 7D, 7E). Interestingly, among the top upstream regulators was CLIC4, an intracellular chloride channel that is required for microvillus assembly in retinal pigmented epithelial cells, where it associates with ezrin and the actin cytoskeleton (Fig. 7E) [35]. A close homolog, CLIC5, is strongly expressed in podocytes and is associated with microvilli and podocalyxin [36]. Collectively, these unbiased experiments suggested critical roles for podocalyxin in regulating cell adhesion and microvillus formation, likely through both direct and indirect pathways.

## DISCUSSION

Podocytes have been challenging to study in culture systems, due to their tendency to dedifferentiate and limited proliferative capacity [15–17]. hPSC-podocytes arise naturally in kidney

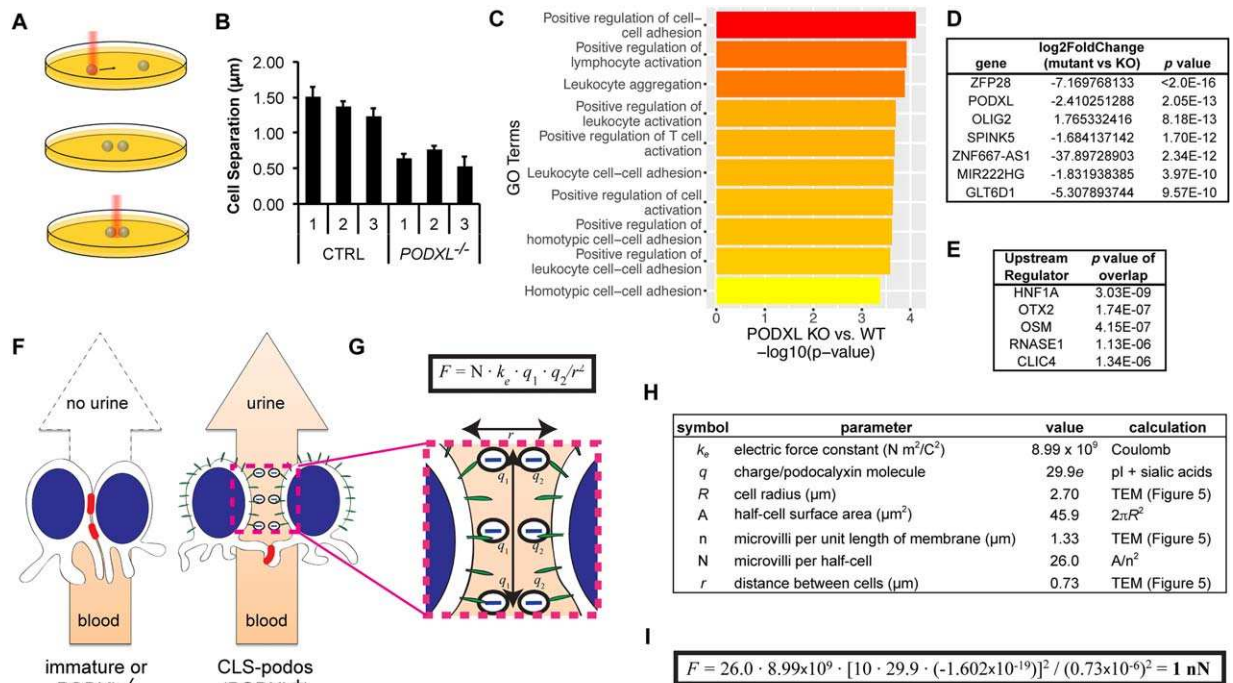


**Figure 7.** Podocalyxin increases cell–cell spacing. **(A):** Schematic representation of optical tweezers experiment. Steps are shown top to bottom. Cells are depicted as green spheres. **(B):** Quantification of gap widths measured with optical tweezers in control or *PODXL*<sup>-/-</sup> cells. Three distinct subclones are shown (average  $\pm$  SEM,  $n \geq 7$  cells per subclone,  $p = 4.39 \times 10^{-17}$ ). **(C):** Top gene ontology terms, **(D)** differentially expressed genes, and **(E)** upstream regulators in *PODXL*<sup>-/-</sup> human pluripotent stem cells, relative to isogenic controls. Data were obtained from three separate experiments (different days), each including 2–3 cell lines of each genotype. **(F):** Schematic representation of podocalyxin function. In the absence of podocalyxin, podocytes remain closely apposed to each other and form lateral junctions through which urine cannot be filtered (left). During capillary loop stage maturation (right), podocalyxin-coated microvilli (green) form on the apical and lateral surfaces of podocytes. Sialic acid residues (negative charges) on podocalyxin act as an anti-adhesive, separating cell membranes and promoting migration of junctional complexes (red) to basal slits, through which urine is filtered. **(G):** Zoom-in of podocyte cell surfaces in close contact, showing the application of Coulomb's law. **(H):** Table of parameters for the estimation of surface area and microvillus charge for each membrane, with **(I)** accompanying electrostatic force calculation for two membranes containing 10 podocalyxin molecules per microvillus. Abbreviations: CLS, capillary loop stage; GO, Gene ontology; KO, knockout; WT, wild type.

organoids in large clusters are therefore an attractive candidate for in vitro studies [3–5, 24]. Although hPSC-podocytes can be clearly discerned within organoids, their appearance and gene expression patterns are different from those of cultured primary and immortalized podocytes [15, 24]. A detailed comparison of hPSC-podocytes to developing podocytes in vivo has not previously been performed, which has made it difficult to determine the developmental stage of these cells and their use in disease modeling and kidney regeneration. Our findings, which directly compare kidney organoids to mouse and human podocytes in tissue sections, reveal that hPSC-podocytes attain a differentiation state and specialized cytoskeletal architecture in cell culture that resembles CLS podocytes in vivo. Gene-edited hPSC-podocytes further reveal ultrastructural defects, which can be recapitulated in transgenic mouse embryos at this stage of development. Thus, perceived differences between organoid hPSC-podocytes and primary podocytes reflect differences in developmental stage or isolation conditions, rather than cell type. Interestingly, our analysis also suggests the presence of transitional cells in-between the podocyte and proximal tubular compartments, which express a distinct combination of markers ( $\text{PAX2}^+ \text{PAX8}^+ \text{LTL}^0 \text{PODXL}^-$ ). The precise identity of these cells is an interesting topic for further investigation.

How podocytes establish their specialized architecture during CLS podocyte maturation is not clear from studies in vivo.

Our TEM analysis reveals for the first time that endogenous podocalyxin is required for efficient microvillus formation in podocytes, both in humans and in mice. Our experiments using optical tweezers further indicate that podocalyxin directly affects the adhesiveness of adjacent cell surfaces in a rapid, context-independent manner. Collectively, these findings suggest a model in which podocalyxin directly induces apical-to-basal junctional migration (Fig. 7F). Podocalyxin localizes to the apical and lateral cell membranes of podocytes, where it induces the localized formation of microvilli via the actin-binding protein ezrin [37, 38]. The strong negative charge on podocalyxin [29] promotes electrostatic repulsion between microvilli on adjacent cells (Fig. 7G). Application of Coulomb's law, together with empirical data from Figure 4 and the literature, reveals that for two cells separated by 0.73  $\mu\text{m}$ , the electrostatic force generated by podocalyxin is  $\sim 1$  nanonewton, and reaches  $\sim 13$  nanonewtons at a distance of 0.2  $\mu\text{m}$  which is typical of *PODXL*<sup>-/-</sup> hPSC-podocytes (Fig. 7H, 7I). These forces are sufficiently strong to repel and separate adjacent cellular membranes from their adhesive interactions [39, 40]. The separation of lateral membranes induces the regional dissolution of cell–cell junctions, which are limited to remaining points of cell–cell contact at the basal membrane. In podocalyxin mutants, repulsion between adjacent membranes is greatly reduced, preventing them from separating and leading

to retention of junctions along their interface and blocked filtration of urine into tubules (Fig. 7F). This model provides novel insight into how junctions are restricted to the basal membranes of podocytes, a critical first step in foot process formation. Anti-podocalyxin antibodies developed for use in cancer and hPSC provide a possible tool for drug delivery or purification of podocytes for therapeutic purposes [41, 42].

A key question is whether kidney organoids and hPSC-podocytes *in vitro* can accurately phenocopy disease states *in vivo*. Our study suggests that loss-of-function mutations in human *PODXL* would likely cause embryonic or perinatal lethality, similar to mice [21]. This might explain why the incidence of podocalyxin mutations in living patients with kidney disease is relatively low [43]. In this regard, our collaborators (laboratories of Drs. Murim Choi and Hae Il Cheong at the Seoul National University College of Medicine, Seoul, Republic of South Korea) recently identified a human neonatal patient with two loss-of-function mutations in *PODXL*—each allele inherited from heterozygous parents. The patient, who unfortunately died at infancy (~ 4 months), presented with severe nephrotic syndrome and omphalocele—characteristics similar to the major defects detected in *Podxl*-deficient mice (Kang et al., manuscript submitted for publication). Thus, both genetic data from patients and our culture assays suggest a highly conserved function for *PODXL* in mammalian development.

Our findings demonstrate that hPSC-podocytes *in vitro* complete the process of junctional migration but do not go on to form bona fide foot processes with tertiary interdigitations. Additional factors are therefore required for podocyte maturation. In this regard, it is striking that hPSC-podocytes form epithelial bilayers that are fused together at their basement membranes. To establish a GBM, one of these podocyte layers must be replaced with a layer of ECs, which may be a key missing factor. Although kidney organoids contain ECs, they are relatively low in abundance, and may lack specialized characteristics required for proper pairing with hPSC-podocytes, such as specific laminin isoform expression [44]. Therefore, an important future direction is to carefully characterize this hPSC-EC compartment and identify ways to further enhance and specialize it to better mimic developing capillary loops *in vivo*.

## CONCLUSION

In conclusion, comparative analysis of hPSC-podocytes *in vitro* and developing CLS podocytes *in vivo* indicates that these are highly similar cell types. Gene-edited hPSC-podocytes reveal

mechanisms of glomerular development at this stage, which are further validated in knockout mice. The accessibility of hPSC-podocytes to experimental manipulation and imaging establishes an attractive model for deciphering the regulatory cues that guide podocyte specialization, with future potential for glomerular regeneration.

## ACKNOWLEDGMENTS

We thank Ed Parker (University of Washington [UW]) for TEM, Ryan Vander werff (University of British Columbia) for transcriptomics, Ryuichi Nishinakamura (Kumamoto University) for NPHS1-GFP cells, and Jonathan Himmelfarb (UW) and Jennifer Harder (University of Michigan) for discussions. This work was supported by NIH National Institute of Diabetes and Digestive and Kidney Diseases K01DK102826 (to B.S.F.); R01DK097598 and UH2DK107343 (to S.J.S.); National Heart, Lung, and Blood Institute K25HL135432 (to H.F.); National Institute of General Medical Sciences P01GM081619 (to Y.W.); Eunice Kennedy Shriver National Institute of Child Health and Human Development R24HD000836 (to Laboratory of Developmental Biology); National Kidney Foundation Young Investigator Grant (to B.S.F.); American Society of Nephrology Carl W. Gottschalk Research Scholar Award (to B.S.F.); Natural Sciences and Engineering Research Council of Canada (RGPIN-155397-13) (to A.W.V.); Directorate for Biological Sciences, National Science Foundation (IDBR DBI-1353718) (to L.Y.L.); and an unrestricted gift from the Northwest Kidney Centers to the Kidney Research Institute.

## AUTHOR CONTRIBUTIONS

Y.K.K., C.R.B., A.J.C., J.W.P., and S.J.S.: performed experiments in human cells and tissues; I.R., A.W.V., M.R.H., and K.M.M.: performed experiments in podocalyxin knockout mice; R.E.G. and N.M.C.: performed experiments in human cells and tissues, performed optical tweezers experiments; P.J., Y.L., and L.Y.L.: performed optical tweezers experiments; Y.W.: performed RNA-Seq analysis; H.F.: performed electrostatic force analysis; B.S.F.: performed experiments in human cells and tissues, performed optical tweezers experiments, performed electrostatic force analysis, performed RNA-Seq analysis, wrote the manuscript with input from all of the authors.

## DISCLOSURE OF POTENTIAL CONFLICTS OF INTEREST

The authors indicated no potential conflicts of interest.

## REFERENCES

- Barak H, Huh SH, Chen S et al. FGF9 and FGF20 maintain the stemness of nephron progenitors in mice and man. *Dev Cell* 2012;22:1191–1207.
- Brown AC, Muthukrishnan SD, Oxburgh L. A synthetic niche for nephron progenitor cells. *Dev Cell* 2015;34:229–241.
- Taguchi A, Kaku Y, Ohmori T et al. Redefining the *in vivo* origin of metanephric nephron progenitors enables generation of complex kidney structures from pluripotent stem cells. *Cell Stem Cell* 2014;14:53–67.
- Takasato M, Er PX, Chiu HS et al. Kidney organoids from human iPSC cells contain multiple lineages and model human nephrogenesis. *Nature* 2015;526:564–568.
- Freedman BS, Brooks CR, Lam AQ et al. Modelling kidney disease with CRISPR-mutant kidney organoids derived from human pluripotent epiblast spheroids. *Nat Commun* 2015;6:8715.
- Dekel B, Burakova T, Arditti FD et al. Human and porcine early kidney precursors as a new source for transplantation. *Nat Med* 2003;9:53–60.
- Xinaris C, Benedetti V, Rizzo P et al. *In vivo* maturation of functional renal organoids formed from embryonic cell suspensions. *J Am Soc Nephrol* 2012;23:1857–1868.
- Unbekandt M, Davies JA. Dissociation of embryonic kidneys followed by reaggregation allows the formation of renal tissues. *Kidney Int* 2010;77:407–416.
- Rogers SA, Lowell JA, Hammerman NA et al. Transplantation of developing metanephroi into adult rats. *Kidney Int* 1998;54:27–37.
- Thomson JA, Itskovitz-Eldor J, Shapiro SS et al. Embryonic stem cell lines derived from

- human blastocysts. *Science* 1998;282:1145–1147.
- 11** Takahashi K, Tanabe K, Ohnuki M et al. Induction of pluripotent stem cells from adult human fibroblasts by defined factors. *Cell* 2007;131:861–872.
- 12** Lam AQ, Freedman BS, Morizane R et al. Rapid and efficient differentiation of human pluripotent stem cells into intermediate mesoderm that forms tubules expressing kidney proximal tubular markers. *J Am Soc Nephrol* 2014;25:1211–1225.
- 13** Morizane R, Lam AQ, Freedman BS et al. Nephron organoids derived from human pluripotent stem cells model kidney development and injury. *Nat Biotechnol* 2015;33:1193–1200.
- 14** Mae S, Shono A, Shiota F et al. Monitoring and robust induction of nephrogenic intermediate mesoderm from human pluripotent stem cells. *Nat Commun* 2013;4:1367.
- 15** Saleem MA, O'hare MJ, Reiser J et al. A conditionally immortalized human podocyte cell line demonstrating nephrin and podocin expression. *J Am Soc Nephrol* 2002;13:630–638.
- 16** Kim YG, Alpers CE, Brugarolas J et al. The cyclin kinase inhibitor p21CIP1/WAF1 limits glomerular epithelial cell proliferation in experimental glomerulonephritis. *Kidney Int* 1999;55:2349–2361.
- 17** Ronconi E, Sagrinati C, Angelotti ML et al. Regeneration of glomerular podocytes by human renal progenitors. *J Am Soc Nephrol* 2009;20:322–332.
- 18** Reeves W, Caulfield JP, Farquhar MG. Differentiation of epithelial foot processes and filtration slits: Sequential appearance of occluding junctions, epithelial polyanion, and slit membranes in developing glomeruli. *Lab Invest* 1978;39:90–100.
- 19** Hartleben B, Schweizer H, Lubben P et al. Neph-Nephrin proteins bind the Par3-Par6-atypical protein kinase C (aPKC) complex to regulate podocyte cell polarity. *J Biol Chem* 2008;283:23033–23038.
- 20** Reiser J, Kriz W, Kretzler M et al. The glomerular slit diaphragm is a modified adherens junction. *J Am Soc Nephrol* 2000;11:1–8.
- 21** Doyonnas R, Kershaw DB, Duhme C et al. Anuria, omphalocele, and perinatal lethality in mice lacking the CD34-related protein podocalyxin. *J Exp Med* 2001;194:13–27.
- 22** Kestila M, Lenkkeri U, Mannikko M et al. Positionally cloned gene for a novel glomerular protein–nephrin—is mutated in congenital nephrotic syndrome. *Mol Cell* 1998;1:575–582.
- 23** Boute N, Gribouval O, Roselli S et al. NPHS2, encoding the glomerular protein podocin, is mutated in autosomal recessive steroid-resistant nephrotic syndrome. *Nat Genet* 2000;24:349–354.
- 24** Sharmin S, Taguchi A, Kaku Y et al. Human Induced Pluripotent Stem Cell-Derived Podocytes Mature into Vascularized Glomeruli upon Experimental Transplantation. *J Am Soc Nephrol* 2016;27:1778–1791.
- 25** Debruin EJ, Hughes MR, Sina C et al. Podocalyxin regulates murine lung vascular permeability by altering endothelial cell adhesion. *PLoS One* 2014;9:e108881.
- 26** Jing P, Wu J, Liu GW et al. Photonic crystal optical tweezers with high efficiency for live biological samples and viability characterization. *Sci Rep* 2016;6:19924.
- 27** Anders S, Huber W. Differential expression analysis for sequence count data. *Genome Biol* 2010;11:R106.
- 28** Alexa A, Rahnenfuhrer J, Lengauer T. Improved scoring of functional groups from gene expression data by decorrelating GO graph structure. *Bioinformatics* 2006;22:1600–1607.
- 29** Kerjaschki D, Vernillo AT, Farquhar MG. Reduced sialylation of podocalyxin—the major sialoprotein of the rat kidney glomerulus—in aminonucleoside nephrosis. *Am J Pathol* 1985;118:343–349.
- 30** Ryan G, Steele-Perkins V, Morris JF et al. Repression of Pax-2 by WT1 during normal kidney development. *Development* 1995;121:867–875.
- 31** Bouchard M, Souabni A, Mandler M et al. Nephric lineage specification by Pax2 and Pax8. *Genes Dev* 2002;16:2958–2970.
- 32** Kann M, Ettou S, Jung YL et al. Genome-wide analysis of Wilms' tumor 1-controlled gene expression in podocytes reveals key regulatory mechanisms. *J Am Soc Nephrol* 2015;26:2097–2104.
- 33** Guo G, Morrison DJ, Licht JD et al. WT1 activates a glomerular-specific enhancer identified from the human nephrin gene. *J Am Soc Nephrol* 2004;15:2851–2856.
- 34** Horrillo A, Porras G, Ayuso MS et al. Loss of endothelial barrier integrity in mice with conditional ablation of podocalyxin (Podxl) in endothelial cells. *Eur J Cell Biol* 2016;95:265–276.
- 35** Chuang JZ, Chou SY, Sung CH. Chloride intracellular channel 4 is critical for the epithelial morphogenesis of RPE cells and retinal attachment. *Mol Biol Cell* 2010;21:3017–3028.
- 36** Wegner B, Al-Momany A, Kulak SC et al. CLIC5A, a component of the ezrin-podocalyxin complex in glomeruli, is a determinant of podocyte integrity. *Am J Physiol Renal Physiol* 2010;298:F1492–F1503.
- 37** Nielsen JS, Graves ML, Chelliah S et al. The CD34-related molecule podocalyxin is a potent inducer of microvillus formation. *PLoS One* 2007;2:e237.
- 38** Takeda T, Go WY, Orlando RA et al. Expression of podocalyxin inhibits cell-cell adhesion and modifies junctional properties in Madin-Darby canine kidney cells. *Mol Biol Cell* 2000;11:3219–3232.
- 39** Krieg M, Arboleda-Estudillo Y, Puech PH et al. Tensile forces govern germ-layer organization in zebrafish. *Nat Cell Biol* 2008;10:429–436.
- 40** Thie M, Rospel R, Dettmann W et al. Interactions between trophoblast and uterine epithelium: Monitoring of adhesive forces. *Hum Reprod* 1998;13:3211–3219.
- 41** Snyder KA, Hughes MR, Hedberg B et al. Podocalyxin enhances breast tumor growth and metastasis and is a target for monoclonal antibody therapy. *Breast Cancer Res* 2015;17:46.
- 42** Choo AB, Tan HL, Ang SN et al. Selection against undifferentiated human embryonic stem cells by a cytotoxic antibody recognizing podocalyxin-like protein-1. *STEM CELLS* 2008;26:1454–1463.
- 43** Barua M, Shieh E, Schlondorff J et al. Exome sequencing and in vitro studies identified podocalyxin as a candidate gene for focal and segmental glomerulosclerosis. *Kidney Int* 2014;85:124–133.
- 44** St John PL, Abrahamson DR. Glomerular endothelial cells and podocytes jointly synthesize laminin-1 and -11 chains. *Kidney Int* 2001;60:1037–1046.



See [www.StemCells.com](http://www.StemCells.com) for supporting information available online.